Numerical Studies of Sampling Efficiencies of the ASCME and PMS Aspirator Hydrometeor Measurement Instruments

HILLYER G. NORMENT

Atmospheric Science Associates, Concord, MA 01742

(Manuscript received 13 June 1986, in final form 26 September 1986)

ABSTRACT

A three-dimensional first-order panel code is used to calculate airflow around and into the Airborne Snow Concentration Measuring Equipment (ASCME), and an axisymmetric second-order panel code is used to calculate flow to and through the Particle Measuring Systems (PMS) Aspirator horn. Air intake by the ASCME inlet tube is taken to be either zero or at the free stream flow rate. Calculations are done for three aspirator horn axis angles relative to horizontal: 27°, 60° and 90°, with a uniform exterior horizontal wind of 2 m s^{-1} along with a fan-induced horn throat airspeed of 12.1 m s^{-1}. The flow codes are combined with three dimensional trajectory codes to calculate hydrometeor fluxes through the sampling volumes of the instruments. Excellent sampling efficiencies for the ASCME are indicated for all flow conditions studied, and for comprehensive size ranges of water drops and hexagonal plate ice crystals.

Convergent flow to the PMS Aspirator measurement volume causes large flux distortions for small waterdrops. Accessibility of larger drops to the measurement volume is dependent on the horn axis angle relative to the horizontal. When they can reach the sampling volume, drops over a wide range of diameters (approximately 40–400 μm) show extreme flux distortions owing to combined effects of flow convergence and the variation of trajectory curvature required for drops to reach all parts of the measurement volume. Finally, large drops are found to pass through the measurement volume at speeds substantially less than the airspeed.

1. The instruments

a. Airborne Snow Concentration Measuring Equipment (ASCME)

The ASCME is a precipitation water content measuring instrument, which is described in detail by Lacombe (1983). In essence, it consists of an inlet tube mounted on a horizontal rotating arm (Figs. 1 and 2). As the arm rotates, hydrometeors in the annular volume swept out by the inlet tube are collected into the inlet tube orifice. A suction is maintained inside the tube such as to eliminate stagnation at its orifice, and thereby enhance collection efficiency.

The outer portion of the arm is covered with an airfoil to reduce drag. Figure 2a shows overall dimensions of the arm, airfoil and inlet tube. The airfoil has a constant cross-section profile (Fig. 2b), which is symmetrical across its chord plane, and the chord plane is horizontal such that significant lift is not generated during rotation. The instrument is positioned at a fixed ground location.

b. Particle Measuring Systems (PMS) Aspirator[1]

The PMS Aspirator consists of a PMS two-dimensional, gray scale, imaging hydrometeor spectrometer mounted in the throat of a flared horn (Fig. 3). Exhaust fans, mounted in the throat downstream of the sampling volume, pull air and hydrometeors through the horn such that they converge to the spectrometer measurement volume. Vanes position the horn such that its mouth faces into the wind, and the horn axis can be adjusted to any angle relative to the horizontal. The instrument records two-dimensional images of individual hydrometeors as they pass through a laser beam. Knowledge of transit velocity is required to be able to reconstruct hydrometeor shapes and sizes from the two-dimensional images. This instrument also is positioned at a fixed ground location. Field application of the instrument with the horn axis pointed vertically is described by Humphries (1985).

2. Flow calculation methods

a. ASCME

For the ASCME a three-dimensional first-order panel code is used to calculate flow (Norment, 1985). This is a modified version of a code developed by Hess (1972). The method is limited to exterior flow, but flow into an orifice can be accommodated. It requires that the body surface be represented by contiguous, plane, quadrilateral panels.

Steady potential flow is calculated for both instrument studies. Thus, effects of turbulence and transient

[1] Particle Measuring Systems, Inc., Boulder, Colorado.

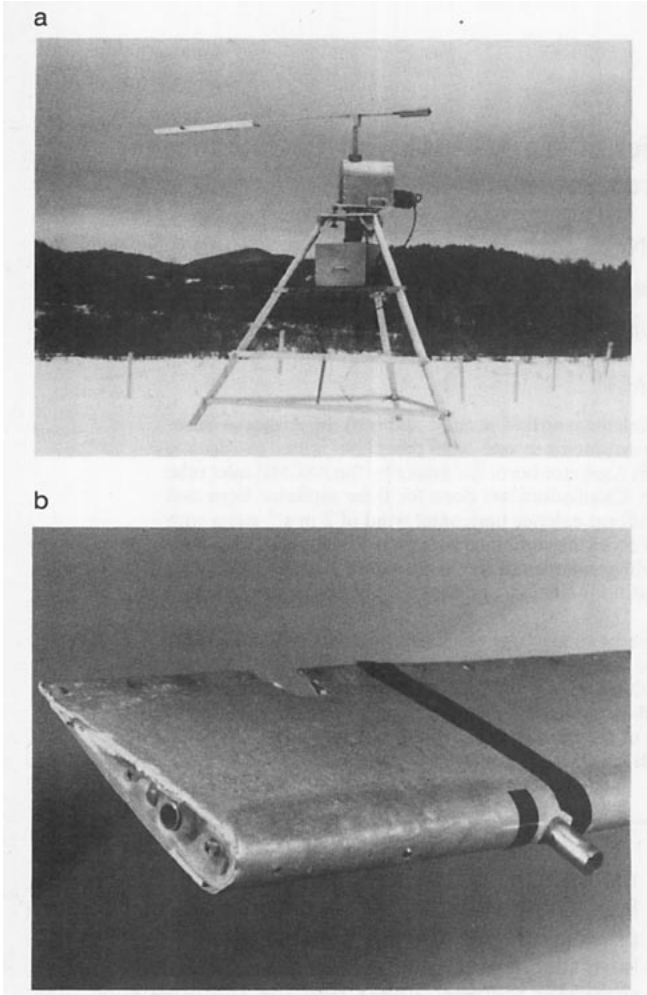

FIG. 1. ASCME precipitation water content instrument. (a) Mounted for field use; (b) airfoil tip and inlet tube.

phenomena, such as wind gusts, are ignored though they may be important. Also ignored are compression and boundary layer effects, but these are not important.

For the types of calculations required here, accuracy has been found to be excellent. Details of many studies are presented by Hess and Smith (1962, 1967).

Panel descriptions of the surfaces of the ASCME airfoil and inlet tube were developed as shown in Fig. 4. Flow calculations were for a single uniform onset flow; variation of onset flow with radial distance from the rotation axis was ignored. This simplification is justified by the fact that drag variation caused by rotation shear on hydrometeors entering opposite sides of the orifice is not significant (less than 3%).

b. PMS Aspirator

First-order panel methods do not give accurate results for interior flows. Therefore, a second-order axisymmetric code developed by Hess and Martin (1974) was adapted for use; see also Friedman (1974).

Aspiration flow, generated by the throat fans, was simulated by use of the surface vorticity method (Hess and Martin, 1974). An exterior onset flow (ambient wind) at any angle relative to the body symmetry axis can be added to the aspiration flow (Hess, 1962).

Figure 5 shows the cross-section profile used to represent the surface of the aspirator horn. Interior surface point coordinates were measured at the U.S. Army Cold Regions Research and Engineering Laboratory (CRREL) and smoothed slightly. Thickness of the horn wall is exaggerated to avoid unwanted interactions between panel end points on the inner and outer surfaces. This greatly improves accuracy of the interior flow, and we assume that it has only a small effect on exterior flow upstream of the horn mouth. Beyond a downstream axis distance of 62 cm from the horn mouth, the throat radius is constant (7.62 cm), and the center of the measurement volume is at 72 cm from the mouth. To ensure calculation of a constant airspeed in the throat (12.1 m s^{-1}), the throat length was extended to 1.5 m from the mouth, and beyond 72 cm was described by points at increments of 3 cm.

Presence of the hydrometeor spectrometer in the throat was ignored since the bulk of the instrument (the canister) is downstream of the exhaust fans, and the only parts that extend upstream are the probe arm tips which would not be expected to affect significantly the flow in most cases.

3. Hydrometeor trajectory calculation method

Trajectories are calculated by use of three-dimensional particle equations of motion that include effects of gravity settling (Norment, 1985). Calculation is started far enough upstream of the body to be essentially in the unperturbed free stream, and the equations of motion are integrated numerically via the code DVDQ of Krogh (1970). Experimental drag data, generalized in terms of Reynolds and Davies numbers, allow highly accurate calculation of trajectories of water drops of diameters up to several hundred micrometers; trajectories of larger drops are calculated with decreasing accuracy up to the break-up size. Similarly trajectories of various ice crystal forms are calculated for somewhat more restricted size ranges (Norment, 1975). Details of a number of accuracy assessments are presented elsewhere (Norment and Zalosh, 1974; Norment, 1980, 1985).

A quantity called concentration factor, C_F, is used as a measure of particle flux distortion caused by interaction of particle inertia with flow perturbations in passing by a body or through an inlet or duct. It is defined for a specified target point, near a body surface or inside an inlet or duct, as

$$C_F = \frac{\text{particle flux at target point}}{\text{particle flux in free stream}} \quad (1)$$

The ratio, C_M, of particle concentration at the target point to free stream concentration is

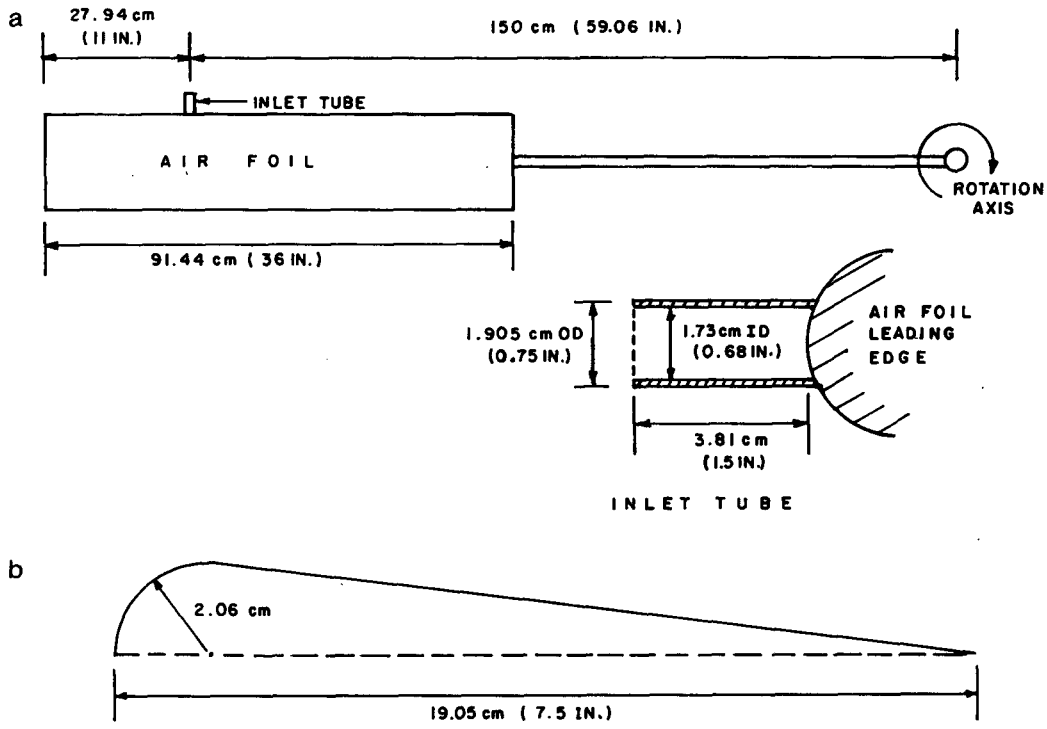

FIG. 2. Scale drawings of the ASCME airfoil and inlet tube. (a) Configuration and dimensions of the complete assembly and inlet tube; (b) airfoil cross section (which is symmetrical across the chord plane).

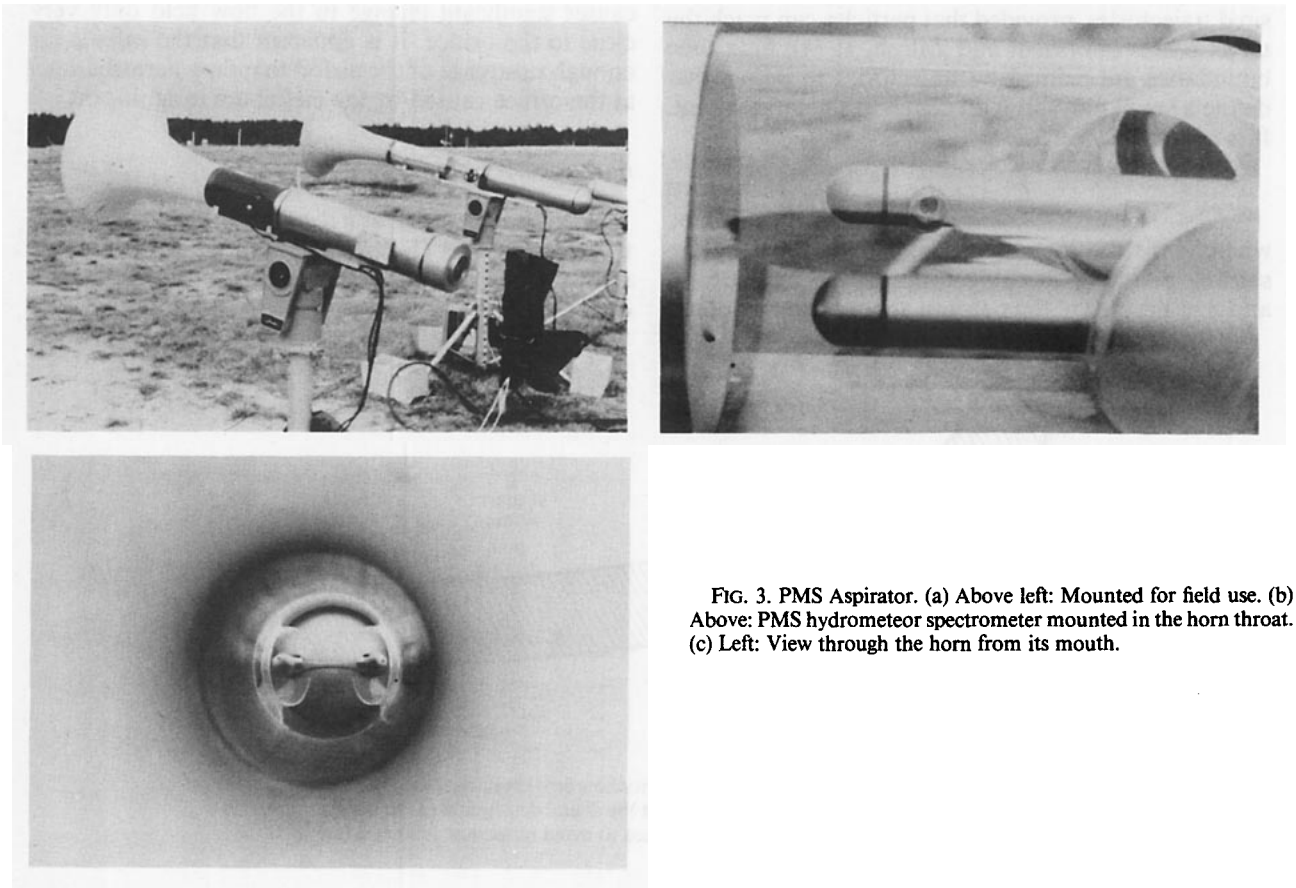

FIG. 3. PMS Aspirator. (a) Above left: Mounted for field use. (b) Above: PMS hydrometeor spectrometer mounted in the horn throat. (c) Left: View through the horn from its mouth.

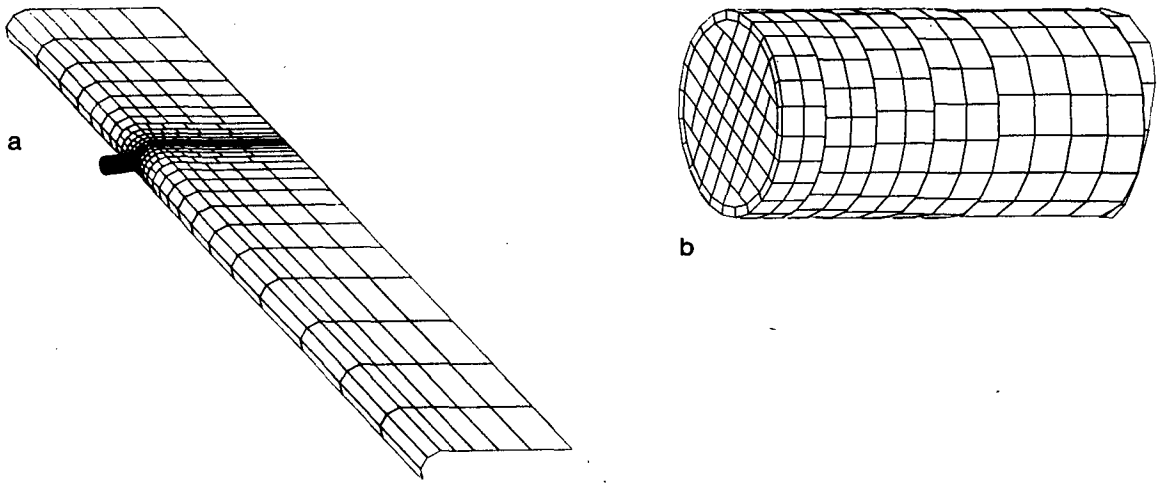

FIG. 4. Panel description of the ASCME airfoil and inlet tube. Each of the inlet tube orifice panels can be made to "leak" a specified fraction of the free stream flow. (a) Complete assembly. The underside of the airfoil is not shown to avoid confusion of overlapping lines; (b) inlet tube.

$$C_M = C_F V / V_{P,t} \quad (2)$$

where V and $V_{P,t}$ are, respectively, free stream airspeed and particle speed at the target point.

To estimate C_F and C_M, the code calculates flux tubes of particles from the undisturbed free stream to the specified target. This is done by use of iterative trajectory calculations that rapidly converge to the desired trajectories, provided that particles can reach the target points (Norment and Zalosh, 1974). Flux tube boundaries are defined by trajectories to points that define a small polygon with center at the target point. It is easy to show that

$$C_F \approx A_{fs}/A_t \quad (3)$$

where A_{fs} is the area of the polygon defined by the starting points of the trajectories in the free stream, and A_t is the area of the polygon about the target point.

4. ASCME results

a. Flow field

Figure 6 shows the flow field about the inlet tube and airfoil with flow into the inlet orifice at the free stream rate; this represents the normal operating specification for the instrument. Zero intake by the inlet causes significant change in the flow field only very close to the orifice. It is apparent that the inlet is far enough upstream of the airfoil that flow perturbations at the orifice caused by the airfoil are insignificant.

b. Trajectory results

With the inlet tube at a distance of 1.5 meters from the rotation axis (Fig. 2) and a rotation rate of 130 rpm, the free stream onset speed is 20.42 m s^{-1}. Other data used are:

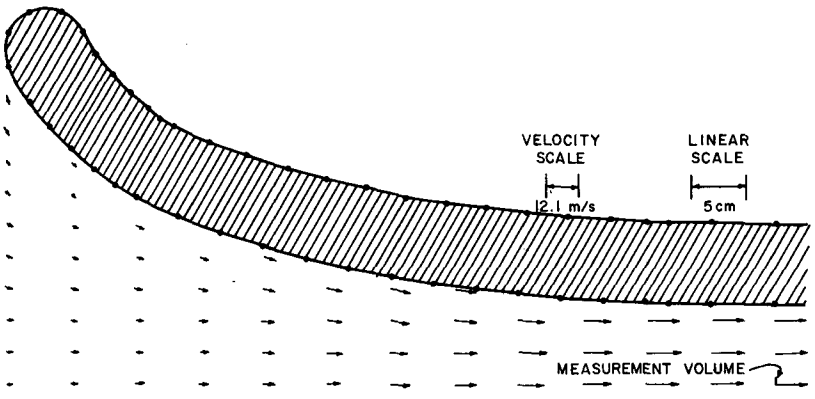

FIG. 5. PMS Aspirator horn profile and interior flow field resulting from aspiration only. The dots are panel end points, which represent the digital description of the horn surface. Thickness of the horn wall is greatly exaggerated to avoid numerical problems (see text).

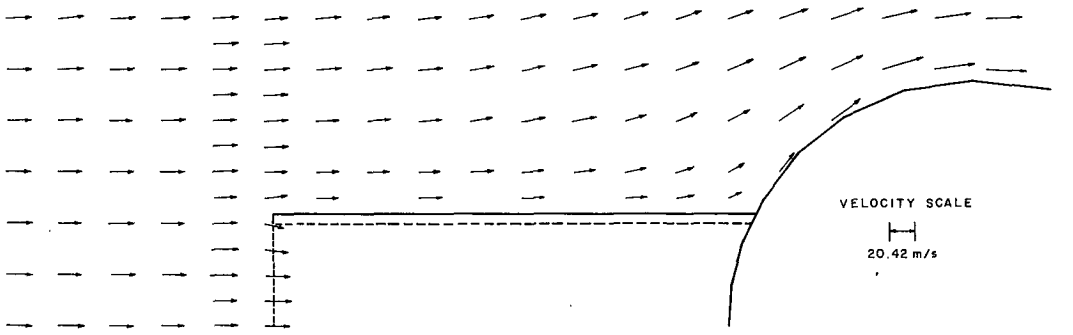

FIG. 6. Airflow into and about the ASCME inlet tube with intake by the inlet orifice at the free stream rate.

Air density $0.984\ \text{kg m}^{-3}$

Air viscosity $1.9696 \times 10^{-5}\ \text{N s m}^{-2}$.

Concentration factors were calculated using six trajectories, with target points evenly spaced around the orifice and very close to its rim, to determine the flux tube boundaries. Figure 7 shows flux tube trajectories, plus the central trajectory, of 200 μm diameter waterdrops to the orifice.

Results for waterdrops are given in Table 1. With the instrument operating according to specification, i.e., with air intake by the orifice at the free stream speed, we calculate essentially isokinetic sampling for water drops of all sizes. This is consistent with the minor influence of the inlet tube and airfoil on flow near the inlet tube orifice shown in Fig. 6 and the straight trajectories shown in Fig. 7. Total air stagnation at the orifice center (zero intake) produces only minor flux distortions for all but the smallest droplets.

The foregoing calculations ignore effects of ambient wind. Since the apparatus is only a few meters above the ground, typical wind speeds would be expected to be small relative to the rotational speed at the orifice. For this reason we would expect the maximum effect to appear when the wind is normal to the inlet tube axis. Calculations were done for a 2 m s^{-1} wind normal to the inlet tube axis, while the rotation induced speed was maintained at 20.42 m s^{-1}. Intake by the orifice was 100% of the rotation-induced free stream speed. Results are not significantly different from those in Table 1 for intake at the free stream rate, which indicates that wind effects are not significant.

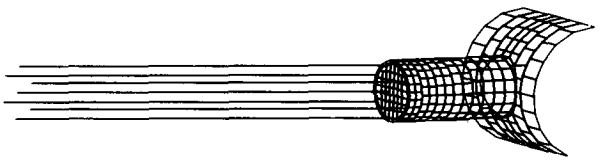

FIG. 7. Portion of the flux tube and central trajectory of 200 μm diameter waterdrops to the ASCME inlet tube orifice. Orifice air intake is at the free stream rate.

Calculations also were done for hexagonal plate ice crystals; results are given in Table 2. Again, the instrument shows essentially isokinetic sampling. Properties of the ice crystals, also given in Table 2, were obtained as explained by Norment (1975).

5. PMS Aspirator results

a. Flow fields

Figure 5 shows the calculated flow field through the horn with no external onset flow. Laboratory measurements of flow speed along the horn axis were made at CRREL with the aspiration fans on and no external onset flow. Comparison of observed with calculated results shows that calculation errors are close to the measurement accuracy, and the maximum error is less than 5%.

Figure 8 shows flow to and through the horn with its axis at an angle of 27° to the horizontal in a 2 m s^{-1} horizontal onset flow (wind). We assume that the horn always orients itself such that its symmetry axis is in a vertical plane, that is, parallel with the onset flow, with mouth facing the flow. Figure 9 is similar for the horn axis at an angle of 90° to the horizontal. Both figures show the vertical plane that contains the horn axis.

TABLE 1. Concentration factors C_F and concentration ratios C_M for waterdrops to the ASCME orifice for extremes of air intake by the orifice.

Waterdrop diameter (μm)	No intake		Intake at the free stream rate	
	C_F	C_M	C_F	C_M
1000	0.972	0.956		
700	0.981	0.977	0.994	0.987
400	0.986	0.993	0.989	0.991
200	0.982	1.003	0.989	0.997
100	0.960	1.016	0.981	1.000
70	0.936	1.029	0.973	1.002
40	0.863	1.066	0.951	1.002
20	0.684	1.227		

TABLE 2. Concentration factor results for hexagonal ice plates to the ASCME orifice. Air intake by the orifice is at the free stream rate.

Plate diameter (μm)	Plate thickness (μm)	Diameter of waterdrops of equal mass (μm)	Mass (μg)	Density (kg m^{-3})	Gravity settling speed (m s^{-1})	C_F	C_M
700	38.26	229	6.29	516	0.333	0.982	1.000
400	29.76	129	1.124	363	0.153	0.971	1.003
200	21.80	67	0.158	278	0.0584	0.950	1.004
100	15.97	~40	3.35×10^{-2}	323	0.0283	0.934	1.001
70	13.61	~31	1.56×10^{-2}	360	0.0191	0.927	0.999
40	10.58	~23	6.37×10^{-3}	579	0.0130	0.922	0.995

b. Trajectory results

The center of the particle measurement volume is in the horn throat at a distance of 72 cm from the horn mouth. A plane normal to the symmetry axis at 72 cm cuts this volume to form a narrow rectangular "measurement area" of dimensions 6.1 cm × 0.62 cm. The long sides of the rectangle are always horizontal. Concentration factors are determined by calculating the four trajectories to the corners of the rectangle.

All of the trajectory calculations were done for a 2 m s^{-1} onset wind and for a throat aspiration speed[2] of 12.1 m s^{-1}. Waterdrop trajectories in a steady unperturbed 2 m s^{-1} wind are shown in Fig. 10; these trajectories are helpful in interpreting the results discussed here. Air density and viscosity were taken to be the same as already given for the ASCME studies.

Trajectories were studied for three horn axis angles relative to the horizontal: 27°, 60° and 90°. The 27° angle is a "typical" value used in the field which represents a compromise between effects of ambient wind and settling speed on hydrometeor trajectory, and thus serves to enhance collection of a particular size and type of hydrometeor. The angles 60° and 90° were chosen arbitrarily to show horn axis angle effects on sampling efficiencies.

1) HORN AXIS AT 27° TO HORIZONTAL

Concentration factor results are listed in Table 3. For waterdrops of diameters 40–200 μm, very large concentration factors are calculated. This is caused, in

[2] Total throat airspeed, including the effect of the onset flow, is slightly higher than 12.1 m s^{-1} when the horn axis is tilted toward the onset flow. Calculated total throat airspeeds are given in Tables 3, 4 and 5.

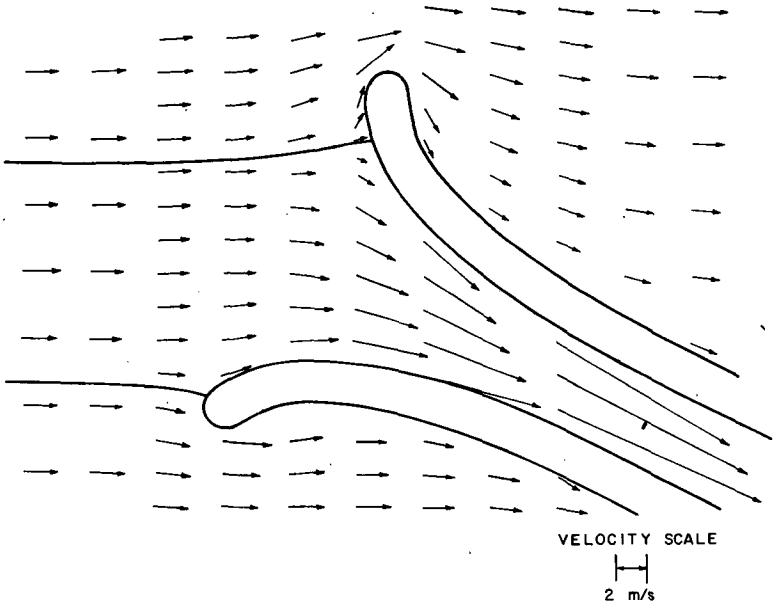

FIG. 8. Airflow in the vertical plane that includes the PMS Aspirator horn axis, which is at an angle of 27° to the horizontal. Throat aspiration speed is specified to be 12 m s^{-1}, and the horizontal crossflow is 2 m s^{-1}. The heavy curves are approximate dividing streamlines between exterior and intake flow.

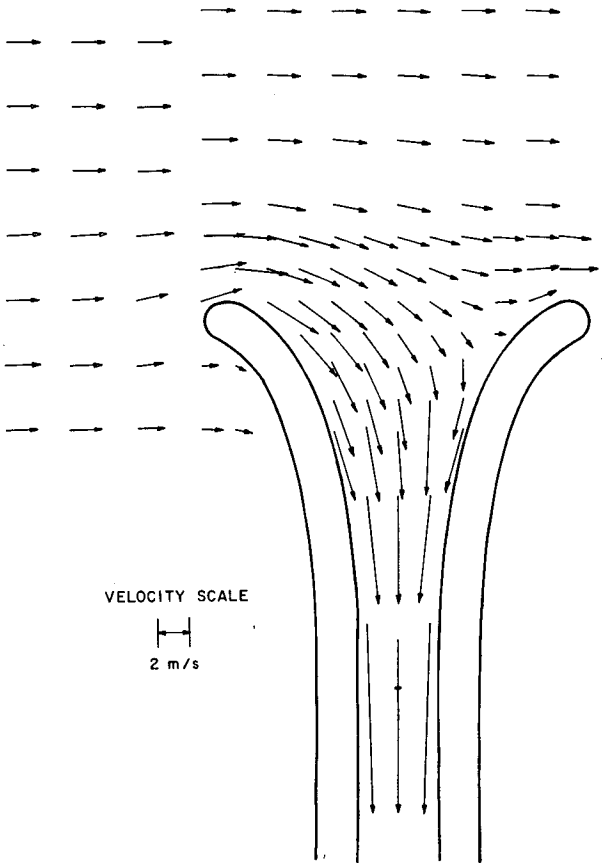

FIG. 9. As in Fig. 8 but with the horn axis at an angle of 90° to the horizontal.

part, by the convergent flow. However, the concentration factor for infinitesimal particles, which would exactly follow the air flow, is only 7.29 (throat air speed/exterior air speed = 14.57/2), and therefore, some additional distorting effect is at work. Figure 11, which shows flux tube trajectories of 200 μm waterdrops to the measurement area, clearly shows the nature of this effect. Since the horn axis is not parallel with the free stream trajectories, the trajectories must bend as they enter the horn, and since the trajectories to the upper side of the measurement area bend more than those to the lower side, additional flux distortion results.

We find that trajectories of 200 μm diameter waterdrops cannot reach all parts of the measurement area. However, concentration factors are obtained for measurement area widths, Δy, less than the maximum value of 6.1 cm, and these results are given in Table 3 and

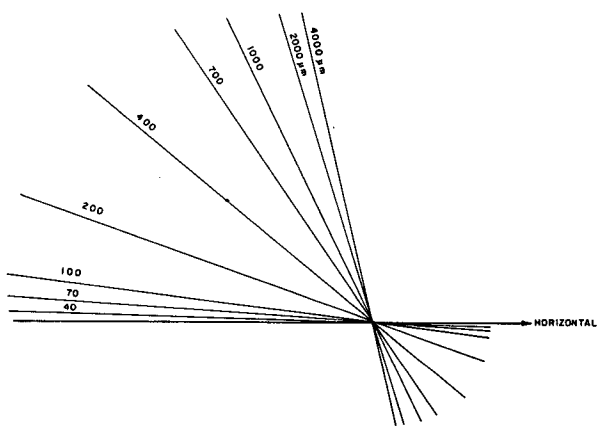

FIG. 10. Free stream (unperturbed) waterdrop trajectories in a uniform horizontal airflow of 2 m s^{-1}.

TABLE 3. Concentration factor results for waterdrops to the PMS aspirator measurement area with horn axis angle at 27° to the horizontal.

Waterdrop diameter (μm)	Δy* (cm)	C_F	C_M	$V_{P,t}$** (m s^{-1})
40	6.1	9.19	1.282	14.34
70	6.1	11.51	1.693	13.60
100	6.1	14.08	2.214	12.72
200	0.62	17.33	3.340	10.38
200	1.525	17.63	3.396	10.38
200	3.053	19.06	3.672	10.38
200	4.2	22.94	4.419	10.38
200	4.575	27.42	5.282	10.38

* Flux tube cross sections in the target plane are rectangles with dimensions $\Delta y \times 0.62$ cm, the rectangle being oriented with long side horizontal. (See Fig. 12.)

** Particle speed at the center of the sampling area. Airspeed at this point is 14.57 m s^{-1}.

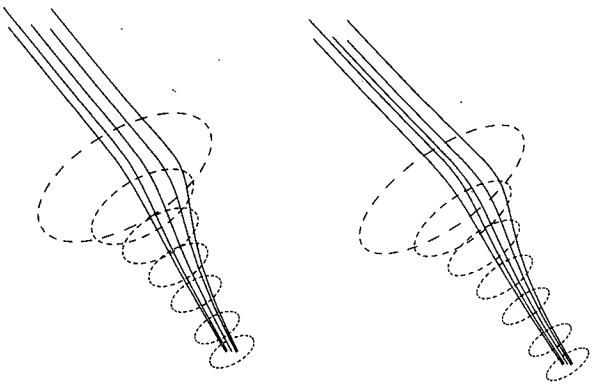

FIG. 11. Stereographic plot of the flux tube and central trajectory of 200 μm waterdrops to the measurement area of the PMS Aspirator. The horn axis is at an angle of 27° to the horizontal, and the flow field is as shown in Fig. 8; Δy = 4.575 cm, C_F = 27.42 (see Table 3 and Figure 12). The dashed-line circles lie on the inside surface of the horn at axial distances from its mouth of: 0, 12, 24, 36, 48, 62 and 72 cm. Three-dimensional perspective can be achieved via use of the crossed-eyes method: Stare at the center of the figure with crossed eyes to make double images of each plot. Adjust the crossing until the centermost images of each member merge. Then concentrate attention on the merged image and you should see the drawing with three-dimensional, stereoscopic perspective.

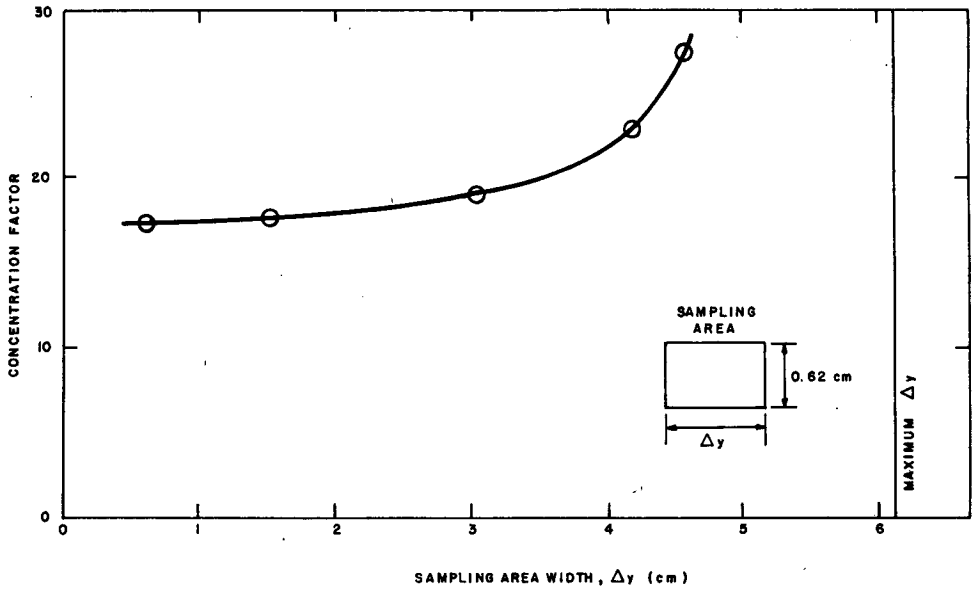

FIG. 12. Concentration factor vs. PMS Aspirator measurement area width for 200 μm diameter waterdrops. Geometry and airflow are as shown in Fig. 8. (See Table 3).

are plotted versus Δy in Fig. 12. The precipitous increase in C_F value as the horn wall is approached is typical of approach to a "shadow zone," which is a region that cannot be reached by the particles. The reason for this is evident in Fig. 11, where with three-dimensional perspective, we see that the trajectories to

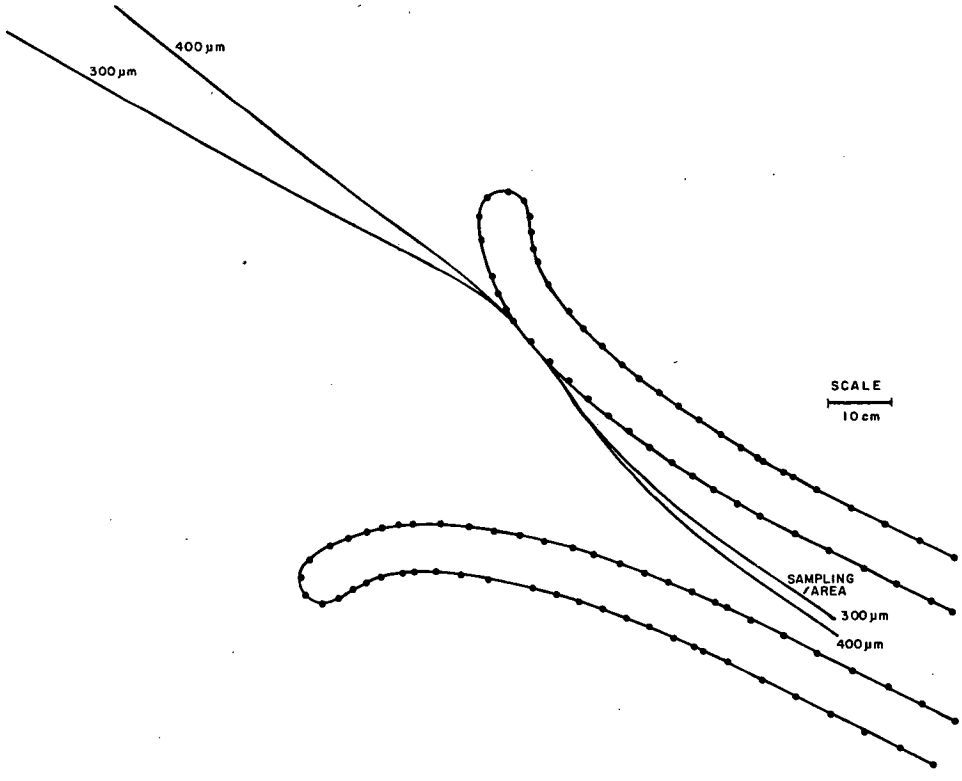

FIG. 13. Trajectories of 300 and 400 μm diameter waterdrops tangent to the upper inside surface of the PMS Aspirator horn in the vertical plane that contains the horn symmetry axis, which is tilted at an angle of 27° to the horizontal. The flow field is as shown in Fig. 8. It is apparent that drops of these sizes cannot reach the sampling area. (See text.)

TABLE 4. Concentration factor results for waterdrops to the PMS aspirator measurement area with horn axis angle at 60° to the horizontal.

Waterdrop diameter (μm)	C_F	C_M	$V_{P,t}$* (m s^{-1})
20	7.104	1.053	13.48
40	8.498	1.277	13.31
70	11.144	1.758	12.68
100	14.256	2.394	11.91
150	20.712	3.877	10.68
200	18.731	3.828	9.79
300	8.203	1.880	8.73
400	4.486	1.125	7.97
700	1.776	0.522	6.81
1000	1.2833	0.383	6.70

* Particle speed at the center of the sampling area. Airspeed at this point is 13.48 m s^{-1}. Measurement area width is 6.1 cm for all cases.

the upper corners of the measurement area pass quite close to the horn wall at an axial distance of about 10 cm from the mouth.

We find that waterdrops of diameters 300 μm and larger can reach no part of the measurement area. This result, at least for 300 μm diameter drops, is surprising in view of the closeness of the drop trajectory angle (30.9°; see Fig. 10) to the horn axis angle (27°). Tangent trajectories (Norment, 1985) of 300 and 400 μm drops to the upper, inside wall of the horn were calculated, and these are shown in Fig. 13. Obviously the regions above the trajectories and downstream of the points of tangency are completely shadowed for these drops; and the shadowed regions include the measurement area. For trajectories not in the central vertical plane, the shadowing would be even more severe.

Thus, for the 27° axis orientation, we find extreme flux distortion for waterdrops smaller than 200 μm in diameter, and the measurement area is calculated to be inaccessible to larger drops.

2) HORN AXIS AT 60° TO HORIZONTAL

Concentration factor results are listed in Table 4 and plotted in Fig. 14. The calculations indicate the measurement area to be accessible to waterdrops up to 1000 μm diameter, but not to 2000 μm and larger drops. Figure 14 indicates that the convergent flow concentration factor limit for infinitesimal particles (6.74) is approached asymptotically as expected.

Drops of intermediate size show large flux distortions, with a peak concentration factor in the neighborhood of 22 or more for diameters between 150 and

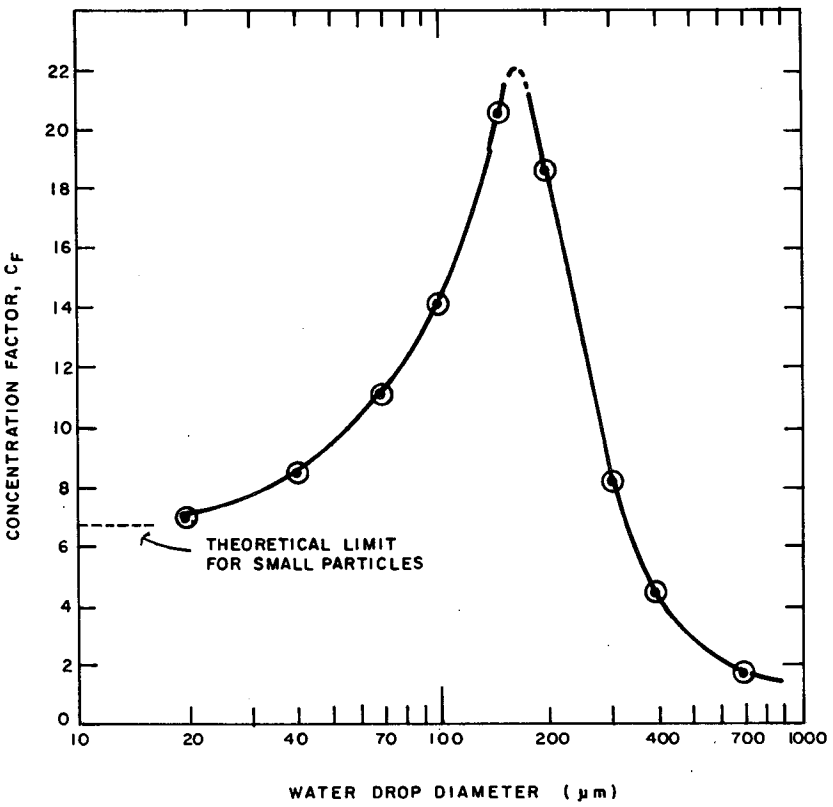

FIG. 14. Concentration factor vs. waterdrop diameter for the PMS Aspirator with its horn axis at an angle of 60° to the horizontal. (See Table 4).

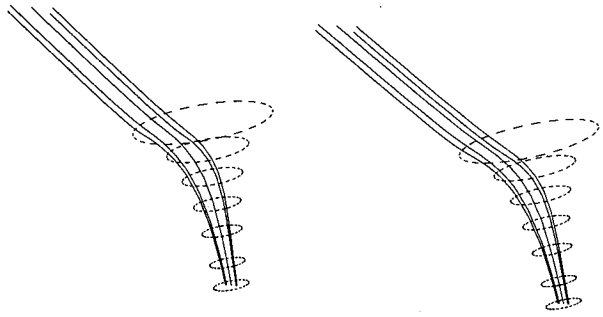

FIG. 15. Stereographic plot of the flux tube and central trajectory of 200 μm diameter waterdrops to the PMS Aspirator measurement area with the horn axis at an angle of 60° to the horizontal. C_F = 18.7. (See Fig. 11 legend.)

TABLE 5. Concentration factor results for waterdrops to the PMS aspirator measurement area with the horn axis angle at 90° to the horizontal.

Waterdrop diameter (μm)	Δy* (cm)	C_F	C_M	$V_{P,t}$** (m s^{-1})
40	6.1	8.02	1.338	11.98
70	3.05	16.48	2.876	11.46
70	4.575	19.89	3.471	11.46
2000				4.10
3000	6.1	1.024	0.213	9.62
4000	6.1	1.014	0.195	10.43

* Flux tube cross sections in the target plane are rectangles with dimensions $\Delta y \times 0.62$ cm, the rectangle being oriented with long side horizontal. (See Fig. 12.)

** Particle speed at the center of the sampling area. Airspeed at this point is 12.1 m s^{-1}.

200 μm. As already discussed, this is the combined result of flow convergence and variations in trajectory curvature required for drops to reach all parts of the measurement area. Comparison of Figs. 11 and 15, show the considerable effect of the axis angle on the flux tube distortions.

3) HORN AXIS AT 90° TO HORIZONTAL

Table 5 gives concentration factor results for the vertical horn orientation. For water droplets of 40 μm diameter, the results are similar to those at the 60° orientation, and Fig. 16 shows a stereoscopic view of the 40 μm droplet flux tube. Droplets of 70 μm diameters could not reach the outer portions of the measurement area. With the measurement area reduced to three fourths of its full width, a concentration factor of almost 20 was calculated. This situation is similar to the one already discussed for 200 μm drops to the horn inclined at 27°.

Drops of 2000 μm diameter can reach some, but not all, parts of the measurement area. Larger drops, which have nearly vertical free stream trajectories (Fig. 10), fall through the horn with little flux distortion.

The measurement area is calculated to be not accessible to drops with diameters between about 70 and 2000 μm.[3]

6. Summary of trajectory results

ASCME. Our calculations indicate that the ASCME should provide nearly ideal sampling of hydrometeors of all sizes. This is especially true when the instrument operates according to the specification that air intake by the inlet tube be close to the free stream flux (which is produced by the arm rotation). However, even if this influx happens to be substantially less than specified, the calculations indicate that sampling efficiency still will be quite satisfactory since sampling of only the smaller hydrometeors will be significantly affected, and these are least important in determining precipitation water content.

PMS Aspirator. For the two-dimensional PMS hydrometeor spectrometers to operate satisfactorily, it is necessary that measurement frequencies be high enough to give adequate sampling statistics, and particle transit velocities through the measurement volume be known. For this reason, aspiration fans are mounted in the horn throat which provide a throat airspeed of about 12 m s^{-1} in the absence of exterior flow. Inevitably, even in the absence of the flared horn, this must cause convergent flow to the measurement volume, and this alone will result in large flux distortions for small hydrometeors.

In addition, we find that when trajectories bend as the particles enter the horn, the bending may vary substantially for trajectories to different portions of the measurement volume such as to produce even more

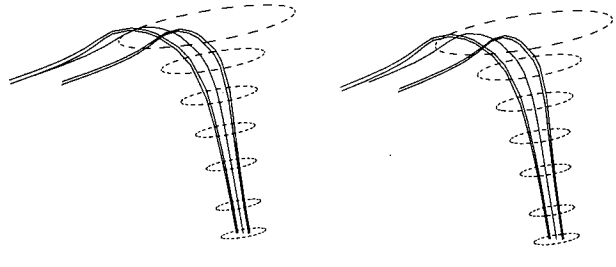

FIG. 16. Stereographic plot of flux tube and central trajectory of 40 μm diameter waterdrops to the PMS Aspirator measurement area with the horn axis at an angle of 90° to the horizontal. C_F = 8.0. (See Fig. 11 legend.)

[3] It is important to realize that steady laminar flow is assumed in the calculations. We would expect the shadowing to be less than complete in practice owing, for example, to effects of turbulence.

serious flux distortion, and this is strongly particle size dependent.

As expected, our calculations indicate that accessibility of large water drops to the measurement volume depends on the angle at which the horn axis is tilted relative to the horizontal and on the exterior onset flow (wind), which was taken to be 2 m s^{-1} for all calculations. At an axis angle of 27°, drops larger than 200 μm in diameter cannot reach the measurement volume for the flow conditions assumed.[4] At a 60° axis angle, only drops with diameters greater than about 1000 μm are completely excluded, but very large flux distortions are calculated for drops with diameters less than about 700 μm. For the horn in a vertical orientation, only very small drops (diameters $\leqslant$ 70 μm) and very large drops (diameters $\geqslant$ 2000 μm) can reach the measurement volume. Small drops (diameters less than about 70 μm), which more closely follow the air streamlines, can reach the measurement volume at any axis angle.

These results show that measurements are sensitive to exterior flow (wind), horn axis angle and hydrometeor size and type, and they imply that the instrument should not be expected to provide accurate sampling across a distribution of hydrometeor types and sizes under the best of conditions. Under realistic field conditions, in turbulent, gusty winds, we would expect correspondingly erratic measurements with additional degradation of accuracy.

Acknowledgments. This work was supported by the U.S. Army Cold Regions Research and Engineering Laboratory, Hanover, NH. We thank Messrs. Roger Berger and James Lacombe for their assistance and guidance.

[4] Effects of turbulence will cause greater accessibility in practice than indicated by the calculations which assume steady, laminar flow.

REFERENCES

Friedman, D. M., 1974: Improved Solution for Potential Flow About Arbitrary Axisymmetric Bodies By Use of a Higher Order Surface Method. Part II. User's Manual for Computer Program, Douglas Aircraft Company, MDC J6627-02, NASA CR 134695. [NTIS N74-33792.]

Hess, J. L., 1962: Calculation of Potential Flow About Bodies of Revolution Having Axes Perpendicular to the Free-Stream Direction. *J. Aerospace Sci.*, **29**, 726–742.

——, 1972: Calculation of Potential Flow About Arbitrary Three-Dimensional Lifting Bodies, Douglas Aircraft Company Rep. No. J5679-01. [NTIS AD-755 480.]

——, and R. P. Martin, 1974: Improved Solution for Potential Flow About Arbitrary Axisymmetric Bodies By Use of a Higher-Order Surface Source Method. Part I. Theory and Results, Douglas Aircraft Company, MDC J6627-01, NASA CR 134694. [NTIS N74-33791.]

——, and A. M. O. Smith, 1962: Calculation of Non-Lifting Potential Flow About Arbitrary Three-Dimensional Bodies, Douglas Aircraft Company Rep. E. S. 40622. [NTIS AD-282 255.]

——, and ——, 1967: Calculation of Potential Flow About Arbitrary Bodies, *Progress in Aeronautical Sciences,* Vol. 8, D. Kuchemann, Ed., Pergammon.

Humphries, J. H., 1985: Application of an Airborne Optical Array Probe for Ground-Based Microphysical Observations. *J. Atmos. Oceanic Technol.*, **1**, 252–259.

Krogh, F. T., 1970: Variable Order Integrators for Numerical Solutions of Ordinary Differential Equations. Jet Propulsion Lab Technology Utilization Document No. CP-2308.

Lacombe, J., 1983: A Technique for Measuring the Mass Concentrations of Falling Snow. *Proc. Int. Soc. of Optical Engineers,* Vol. 414, 17–28.

Norment, H. G., 1975: Effects of Airplane Flow Fields on Cloud Water Content Measurements. Mt. Auburn Research Associates, AFCRL-TR-75-0231. [NTIS AD-A014 807.]

——, 1980: Calculation of Water Drop Trajectories To and About Arbitrary Three-Dimensional Bodies in Potential Airflow, Atmospheric Science Associates, NASA CR 3291. [NTIS N80-28302.]

——, 1985: Calculation of Water Drop Trajectories To and About Arbitrary Three-Dimensional Lifting and Nonlifting Bodies in Potential Airflow. Atmospheric Science Associates, NASA CR 3935. [NTIS N87–11694/3/6AR]

——, and R. G. Zalosh, 1974: Effects of Airplane Flow Fields on Hydrometeor Concentration Measurements. Mt. Auburn Research Associates, AFCRL-TR-0602. [NTIS AD-A006 690.]